Acta Cryst. (1980). A**36**, 178–182

Study of Point-Defect Aggregates in Nearly Perfect Silicon Single Crystals using a High-Resolution Diffuse X-ray Scattering Technique

BY KRISHAN LAL AND BHANU PRATAP SINGH

National Physical Laboratory, Hillside Road, New Delhi 110012, *India*

(*Received* 19 *February* 1979; *accepted* 25 *September* 1979)

Abstract

High-resolution diffuse X-ray scattering (DXS) measurements have been made on dislocation-free silicon single crystals of the following types: (1) as-grown specimen with no heat treatment (labelled as NHT); (2) specimen heated at 1273 K under oxygen for 10 h [labelled as HT(1)] and (3) specimen heated at 1273 K under oxygen for 50 h [labelled as HT(2)]. Reciprocal space around the 111 reciprocal-lattice point in (1,−1,1) geometry has been explored using a Cu $K\alpha_1$ exploring beam. From the distribution of DXS intensity it was found that for sample NHT, the observed DXS is predominantly due to aggregates of vacancies. Heating the specimen under oxygen produces defect aggregates of interstitial type. Infrared absorption measurements showed that the area under the 9 μm absorption band decreases, suggesting that oxygen ions aggregate into clusters of interstitial type. Transmission X-ray topographs also support these results.

1. Introduction

The presence of even a small number of defects in otherwise nearly perfect single crystals is known to have a strong influence on their properties. Therefore, the perfqrmance of electronic devices fabricated out of single crystals of semiconducting materials is significantly influenced by lattice imperfections. Line defects like dislocations can be observed and studied in a non-destructive fashion by X-ray diffraction topographic techniques. Strain produced by point defects and their aggregates is too small to produce appreciable extinction contrast in X-ray topographs. Even when a weak contrast is produced it is not possible to characterize in detail the defect aggregates. On the other hand, it is expected that these defects will produce diffuse X-ray scattering (DXS) from regions of reciprocal space close to a reciprocal-lattice point (relp) (Krivoglaz, 1969; Dederichs, 1971). Therefore, a study of DXS intensity around a relp can give information about point defects and their aggregates (Dederichs, 1973; Peisl, 1975, 1976; Patel, 1975; Lal & Singh, 1977; Lal, 1978; Lal, Singh & Verma, 1979).

Recently, we have developed a technique for the high-resolution measurement of DXS (Lal & Singh, 1977; Lal, 1978; Lal, Singh & Verma, 1978). In this technique a highly collimated $K\alpha_1$ X-ray beam is used as the exploring beam. DXS measurements are made by rotating the crystal by a few seconds of arc from the exact Bragg diffraction condition and by suitably positioning the detector. This technique has been successfully used in making detailed investigations on dislocation-free silicon single crystals (Lal, Singh & Verma, 1979). In this investigation it was found that the nature of the DXS distribution around a relp is very sensitive to the thermal history of the specimen. It is known that a small concentration of oxygen is present in silicon crystals, particularly in those grown from quartz crucibles (Kaiser, Keck & Lange, 1956; Kaiser & Keck, 1957). In silicon-device technology oxidation of silicon at elevated temperatures is an important processing step. Earlier work has shown that defect clusters containing oxygen are produced when silicon crystals containing a small concentration of oxygen are heated at about 1273 K (Patel & Batterman, 1963; Patel, 1973). In the present investigation we have used a high-resolution DXS technique to study the aggregates of oxygen in silicon crystals containing a small concentration of oxygen (Lal, Singh & Schwuttke, 1978; Lal, Singh, Verma & Schwuttke, 1978). Oxygen has also been observed with the help of the infrared absorption around 9 μm. Transmission X-ray topographs of wafers from the adjoining regions of the same boule on which DXS measurements were made were also recorded. In this paper we report the results of these investigations.

2. Experimental

As mentioned above, the DXS measurements have been made by using a recent high-resolution technique. In this technique a triple-crystal X-ray diffractometer (Lal & Singh, 1977; Lal, 1978; Lal, Singh & Verma, 1978; Lal & Singh, 1979) is used. A Hilger Y31 micro-

0567-7394/80/020178-05$01.00

focus X-ray generator with a spot size of 40 μm diameter on the anode is used as a source of X-rays. The X-ray beam from this source is collimated and monochromated by diffraction from a set of two crystals cut in the (1,−1) setting with their diffracting surfaces parallel to (111). The small size of the X-ray source and the use of a special collimator reduces the divergence of the X-ray beam incident on the monochromators to less than 1′ of arc in the horizontal plane. Because of this it is possible to resolve the $K\alpha_1$ X-ray beam which is used as the exploring beam for the specimen. Its divergence in the horizontal plane is much less than 5″ of arc. The specimen and the detector are mounted on a special turntable by which rotations of the order of 1″ of arc can be given to the specimen and the detector.

In the present investigation a Cu $K\alpha_1$ exploring beam was used. Its intensity I_o can be measured accurately. A scintillation counter having a crystal of NaI : Tl as a scintillator is used for intensity measurement. A counting system manufactured by M/s Electronic Corporation of India Ltd, Hyderabad, was used.

The specimen crystals were cut from boules grown along [111]. Their surfaces were parallel to (111) and were ground and lapped to such an extent that no surface damage was left. Wafers for X-ray topographic work were ~1 mm thick whereas crystals for DXS measurements were ~10 mm thick. All these crystals were about 65 mm in diameter. Standard techniques were used for measuring infrared absorption and recording transmission X-ray topographs.

3. Results

Typical results in respect of the following three types of crystals will be discussed: (1) as-grown crystals with no heat treatment, (2) crystals heated for 10 h under oxygen at 1273 K and (3) crystals heated for 50 h under oxygen at 1273 K. For convenience of description we have labelled the crystals under these three categories as NHT, HT(1) and HT(2), respectively.

The infrared absorption band at 9 μm was recorded for all the specimens and the concentration of oxygen attached to the Si ions was determined from the shape of this band (Kaiser, Keck & Lange, 1956; Kaiser & Keck, 1957). It was observed that the concentration of oxygen responsible for this band decreased as a result of the heat treatment. The concentration of oxygen was $1{\cdot}7 \times 10^{15}$, $1{\cdot}6 \times 10^{15}$ and $1{\cdot}5 \times 10^{15}$ atoms mm^{-3} for samples NHT, HT(1) and HT(2), respectively. This suggested that the oxygen responsible for the 9 μm band reduces in concentration as a result of heat treatment.

Transmission X-ray topographs of the NHT samples showed the absence of contrast due to line defects as well as point-defect aggregates. Fig. 1(*a*) is a typical topograph of a NHT crystal. The presence of point-defect aggregates can be detected in X-ray diffraction topographs (Schwuttke, 1962, 1970). In the topographs of samples HT(1) and HT(2) a weak contrast was observed which may be due to strains produced by point-defect aggregates. Fig. 1(b) shows a typical topograph of the specimen HT(2). In Fig. 1(*b*) appreciable contrast is observed near the middle of the topograph. The strain produced by the defects is radial, as can be inferred from the usual topographic contrast condition (Lal & Mader, 1976). The topographs of sample HT(1) also showed similar contrast but it was not as strong as in Fig. 1(*b*).

Fig. 2 shows typical diffraction curves of the samples NHT, HT(1) and HT(2) recorded for the 111 reflection on the triple-crystal X-ray diffractometer. It can be seen that fairly narrow diffraction curves are obtained for all the samples. However, the narrowest curve (half-width 14″ of arc) is for the sample NHT having no heat

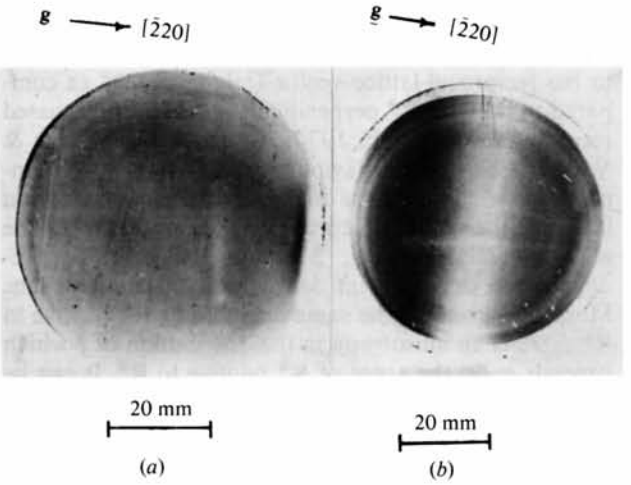

Fig. 1. Typical X-ray projection topographs of samples of types (*a*) NHT, and (*b*) HT(2). Contrast due to point-defect aggregates can be seen in (*b*).

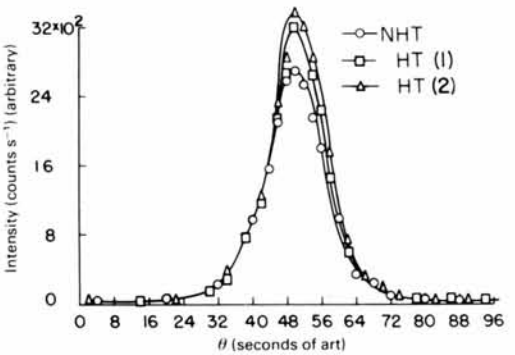

Fig. 2. Typical diffraction curves for the 111 relp of dislocation-free Si single crystals of types NHT, HT(1) and HT(2). Cu $K\alpha_1$ was used as the exploring beam.

treatment. The half-width increased slightly with increase in the time of heating under oxygen. Also, a slight increase in the height of the diffraction curve is observed with the time of oxygen treatment. In this experiment the intensity of the exploring X-ray beam was kept constant ($5{\cdot}9 \times 10^3$ counts s^{-1}) for all the samples. In Fig. 2 the three curves nearly coincide on the left-hand side but do not coincide on the right-hand side. As will be shown later (*Discussion*) this is a result of the creation of oxygen aggregates during heat treatment.

Fig. 3 shows a typical intensity of DXS I *vs* $1/K^{*2}$ plot for a sample of type NHT. **K*** is a vector which joins the centre of the elemental volume of the reciprocal space under investigation to the nearest relp (111 in the present case). The value of the intensity of the exploring beam I_o is $5{\cdot}9 \times 10^3$ counts s^{-1}. It is the same for this and the other DXS measurements (Figs. 4 and 5) as well as for the recording of the diffraction curves (Fig. 2). The results in Fig. 3 correspond to measurements made along four different directions of **K***, namely [111], [$\bar{1}\bar{1}\bar{1}$], [0$\bar{1}$1] and [01$\bar{1}$]. These plots show that for any value of $|\mathbf{K}^*|$, I is very high for **K*** parallel to the reciprocal-lattice vector (rel vector) **R*** as compared to that for **K*** perpendicular to **R***. As discussed recently (Lal & Singh, 1977; Lal, 1978; Lal, Singh & Verma, 1979) this behaviour is because at room temperature in silicon there is no significant contribution from the thermal DXS to the observed value of I. The observed DXS in Fig. 3 is considered to be predominantly due to point defects and their aggregates. Moreover, even for the same direction of **K*** relative to **R*** there is an anisotropy in the distribution of I which depends upon the sense of **K*** relative to **R***. It can be seen that when **K*** is parallel to **R***, for a given value of $|\mathbf{K}^*|$, I has a higher value when **K*** is parallel to [$\bar{1}\bar{1}\bar{1}$] as compared to its value when **K*** is along [111]. This behaviour also strongly suggests that the observed results are predominantly due to defect aggregates.

The above results can be more conveniently described in direct space in terms of the grazing angle θ and the Bragg angle θ_B rather than in reciprocal space in terms of the sense of **K*** relative to **R***. When $\theta > \theta_B$, in reciprocal space it means that **K*** is parallel to **R***. Conversely, when $\theta < \theta_B$, **K*** is antiparallel to **R***. Similarly, θ is greater than θ_B when **K*** is along [0$\bar{1}$1] and θ is less than θ_B when **K*** is along [01$\bar{1}$]. In terms of relative values of θ and θ_B it can be seen that the DXS intensity I is much higher for $\theta < \theta_B$ than for $\theta > \theta_B$ (Fig. 3). Such behaviour is expected if defect aggregates of vacancy type are present in the sample (Dederichs, 1971, 1973; Peisl, 1976). Fig. 3 also shows that I *vs* $1/K^{*2}$ plots are not single straight lines for any direction of **K***. The slope changes at specific values of $|\mathbf{K}^*|$. This behaviour will be discussed after describing the results obtained for samples HT(1) and HT(2) (*Discussion*).

Fig. 4 shows a typical I *vs* $1/K^{*2}$ plot for sample HT(1). The general features of these plots are similar to those shown in Fig. 3. However, it can be seen that heating under oxygen has a remarkable influence on the distribution of I around the relp for small values of $|\mathbf{K}^*|$. In this case it can be seen that, for a given value of $|\mathbf{K}^*|$, the DXS intensity is higher when **K*** is along [111] than when **K*** is along [$\bar{1}\bar{1}\bar{1}$]. This means that the DXS intensity is higher when $\theta > \theta_B$ than when $\theta < \theta_B$. This result is the reverse of the results reported in Fig. 3 for the sample NHT.

Fig. 5 shows typical I *vs* $1/K^{*2}$ plots for sample HT(2). The general features of these plots are similar to those reported for samples NHT and HT(1). In finer details these results are similar to those reported in Fig. 4 for sample HT(1). In this case also it can be observed that the DXS intensity is much higher for $\theta > \theta_B$ than for $\theta < \theta_B$ at small values of $|\mathbf{K}^*|$.

For a given value of $|\mathbf{K}^*|$ the difference between the DXS intensity for measurements with $\theta > \theta_B$ and $\theta < \theta_B$ can be termed as anisotropy in the DXS intensity distribution. It should be noted that only the sense of

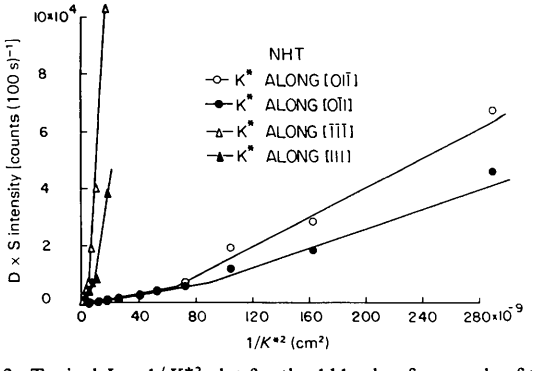

Fig. 3. Typical I *vs* $1/K^{*2}$ plot for the 111 relp of a sample of type NHT. DXS measurements were made for **K*** along [111], [$\bar{1}\bar{1}\bar{1}$], [0$\bar{1}$1] and [01$\bar{1}$]. Cu $K\alpha_1$ was used as the exploring beam.

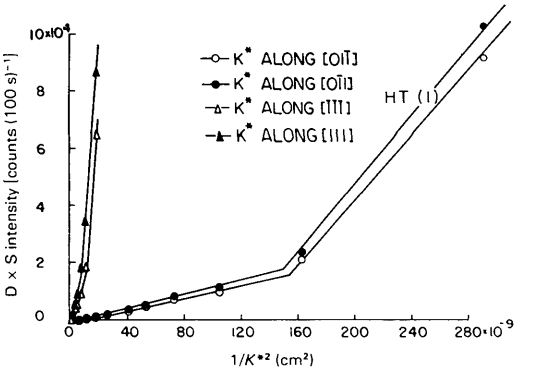

Fig. 4. Typical I *vs* $1/K^{*2}$ plot for the 111 relp of a sample of HT(1). DXS measurements were made for **K*** along [111], [$\bar{1}\bar{1}\bar{1}$], [0$\bar{1}$1] and [01$\bar{1}$]. Cu $K\alpha_1$ was used as the exploring beam.

K* is changed from the $\theta < \theta_B$ to the $\theta > \theta_B$ settings. In other words, for a given $|\mathbf{K}^*|$, we can define

$$\text{anisotropy} = \text{DXS } I_{\theta > \theta_B} - \text{DXS } I_{\theta < \theta_B} \qquad (1)$$

for a given direction of **K***.

Fig. 6 shows a plot of the anisotropy as a function of **K*** for all measurements on all specimens. It can be seen that the anisotropy is much higher when **K*** is along **R*** than when **K*** is perpendicular to **R***. However, even when **K*** is perpendicular to **R*** the sign of the anisotropy changes in the same fashion with heat treatment as the change of sign of anisotropy for **K*** along **R***.

4. Discussion

The results reported for samples NHT show that in the as-grown crystals there are no line defects (Fig. 1*a*). However, an appreciable concentration of oxygen, as revealed by the infrared absorption band at 9 μm, is observed. The distribution of the DXS intensity around the 111 relp is similar to that expected from defect clusters of vacancy type. The anisotropy is negative for all values of $|\mathbf{K}^*|$ (Fig. 6). It can be seen that the anisotropy is very sensitive to the heat treatment given to the specimen. Such behaviour has been observed even for the as-grown samples having slightly different thermal histories (Lal, Singh & Verma, 1979).

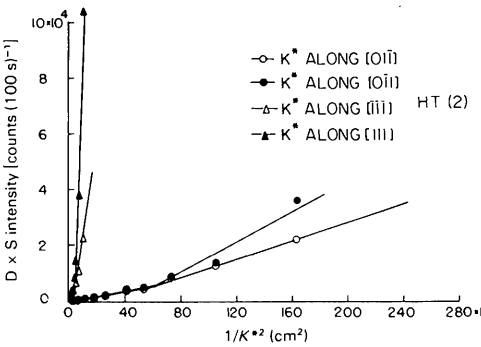

Fig. 5. Typical I *vs* $1/K^{*2}$ plot for the 111 relp of a sample of type HT(2). DXS measurements were made for **K*** along [111], [$\bar{1}\bar{1}\bar{1}$], [01$\bar{1}$] and [0$\bar{1}$1]. Cu $K\alpha_1$ was used as the exploring beam.

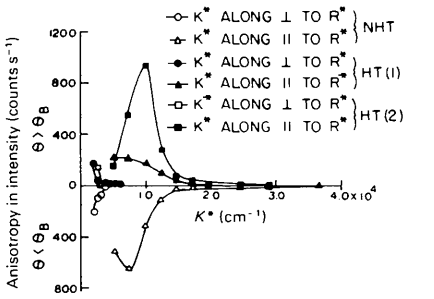

Fig. 6. A plot of the anisotropy in the DXS intensity as a function of $|\mathbf{K}^*|$ around the 111 relp for the samples of types NHT, HT(1) and HT(2). Here anisotropy is defined as [DXS $I_{\theta > \theta_B}$ − DXS $I_{\theta < \theta_B}$] for a given value of $|\mathbf{K}^*|$ and for a given direction of **K***.

Heating under oxygen shows appreciable effects in the infrared absorption at 9 μm, the transmission X-ray topographs and the DXS intensity distribution. The area under the infrared absorption band decreases with the time of heat treatment. This behaviour is consistent with the earlier results (Patel & Batterman, 1963; Patel, 1973, 1975) and is expected to be due to clustering of part of the dissolved oxygen. The present investigation aims at understanding the nature of defect clusters produced by heat treatment.

As is apparent in the preceding section, DXS is well suited for the study of the effect of heat treatment on Si single crystals. The clustering of oxygen is supported by the IR absorption measurement around 9 μm, the X-ray topographic observations and the DXS measurements. The change in the nature of the anisotropy in DXS measurements promises to be a direct method for observing the change in the nature of defect aggregates. This behaviour is also implicit in the diffraction curves of the three samples (Fig. 2). In Fig. 2 it was seen that on the left-hand side the three curves coincide, whereas on the right-hand side the curves are separate. The right-hand side in Fig. 2 corresponds to $\theta > \theta_B$ and, therefore, the increase in intensity for a given value of θ with heat treatment may be a result of the formation of defects of interstitial type. Further, there is a slight increase in the area under the diffraction curves as a result of heat treatment. This may be due to X-ray scattering by interstitial defects.

Having established the nature of the defect clusters on heat treatment under oxygen one is tempted to deduce the size and shape parameters of the defect aggregates. At present no rigorous theoretical formulation is available for analysing this type of data. Some phenomenological models (Dederichs, 1971, 1973; Trinkaus, 1971, 1972) have been developed recently, extending and elaborating the work of Krivoglaz (1969). According to these models the DXS intensity is dependent on different powers of $|\mathbf{K}^*|$, *i.e.*

$$\text{DXS } I = |\mathbf{K}^*|^{-n}, \qquad (2)$$

in different ranges of $|\mathbf{K}|$ values. We have analysed our data by plotting DXS I as a function of **K*** on a log–log plot. Such a plot is very useful in revealing regions of different values of n in equation (2). It was found that the value of n is not an integer most of the time. Its value ranges from about 1 to about 6.

Another important parameter is the value of $|\mathbf{K}^*|$ at which the value of n changes in log DXS I *vs* log $|\mathbf{K}^*|$ plots. Following the convention adopted in our previous work (Lal, Singh & Verma, 1979) we have designated these points as the knee points. Table 1 gives the values of $|\mathbf{K}^*|$ corresponding to different knee

points observed in the entire DXS data. It can be seen that in all there are 48 knee points distributed around seven values of $|\mathbf{K}^*|$. The knee points given in Table 1 are also observed in linear plots (Figs 3, 4 and 5). It can be seen that except for the knee point around $9{\cdot}5 \times 10^3$ cm^{-1} ($\sim 10^4$ cm^{-1}) all the other knee points are observed in all the samples. The knee point at $\sim 10^4$ cm^{-1} is absent in sample HT(1). It is observed in sample NHT for $\mathbf{K}^*$ along [111] and [$\bar{1}\bar{1}\bar{1}$]. However, in sample HT(2) it is observed for all the directions of $\mathbf{K}^*$. The presence of this knee point in sample NHT may be due to clusters of vacancy type having approximately the same size. It may be mentioned that it is around the same value of $|\mathbf{K}^*|$ ($\sim 1 \times 10^4$ cm^{-1}) that the anisotropy shows a peak in Fig. 6 for sample HT(2). This value of $|\mathbf{K}^*|$ corresponds to a size factor of $\sim 10^4$ Å in real space. The value may be treated as the average cluster radius. Since for a given value of $|\mathbf{K}^*|$ the DXS I is much higher for $\mathbf{K}^*$ parallel to than for $\mathbf{K}^*$ perpendicular to the rel vector, it can be concluded that these clusters are platelets located on {111} and that they produce considerable strain in these planes.

It is interesting to note that some of the knee points reported here were also observed in samples used in the preceding investigations (Lal, Singh & Verma, 1979) even though the specimens used here were from entirely different boules. For example, in the earlier specimen knee points were observed at 2×10^3, 3×10^3, 2×10^4 and 3×10^4 cm^{-1}.

Table 1. *Values of* $|\mathbf{K}^*|$ *for different knee points*

Serial number	Position of the knee points (cm^{-1})	Sample	Direction of $\mathbf{K}^*$	Number of knee points
1	$1{\cdot}8 \times 10^3$	NHT HT(1) HT(2)	[0$\bar{1}$0], [01$\bar{1}$]	6
2	$3{\cdot}5 \times 10^3$	NHT HT(1) HT(2)	[0$\bar{1}$1], [01$\bar{1}$]	6
3	$4{\cdot}5 \times 10^3$	NHT HT(1) HT(2)	[0$\bar{1}$1], [01$\bar{1}$]	6
4	7×10^3	NHT HT(1) HT(2)	[111], [$\bar{1}\bar{1}\bar{1}$] [0$\bar{1}$1],]01$\bar{1}$]	12
5	$9{\cdot}5 \times 10^3$	HT(2) NHT	[111], [$\bar{1}\bar{1}\bar{1}$] [0$\bar{1}$1], [01$\bar{1}$]	6
6	$1{\cdot}5$–$1{\cdot}7 \times 10^4$	NHT HT(1) HT(2)	[111], [$\bar{1}\bar{1}\bar{1}$]	6
7	3×10^4	NHT HT(1) HT(2)	[111], [$\bar{1}\bar{1}\bar{1}$]	6

The authors are grateful to Dr A. R. Verma for many valuable discussions and critical comments on this manuscript. The authors are also grateful to Dr G. H. Schwuttke for supplying the specimen used in this investigation together with their topographs and infrared spectra and for his comments on this manuscript.

References

DEDERICHS, P. H. (1971). *Phys. Rev. B*, **4**, 1041–1050.

DEDERICHS, P. H. (1973). *J. Phys. F*, **3**, 471–496.

KAISER, W. & KECK, P. H. (1957). *J. Appl. Phys.* **28**, 882–887.

KAISER, W., KECK, P. H. & LANGE, C. F. (1956). *Phys. Rev.* **101**, 1264–1268.

KRIVOGLAZ, M. A. (1969). *Theory of X-ray and Thermal Neutron Scattering by Real Crystals*. New York: Plenum.

LAL, K. (1978). *Advances in Crystallography*, edited by R. SRINIVASAN, pp. 136–158. Oxford, New Delhi: IBH Publishng Co.

LAL, K. & MADER, S. (1976). *J. Cryst. Growth*, **32**, 357–362.

LAL, K. & SINGH, B. P. (1977). *Solid State Commun.* **22**, 71–74.

LAL, K. & SINGH, B. P. (1979). *Indian J. Phys.* **53A**, 72–77.

LAL, K., SINGH, B. P. & SCHWUTTKE, G. H. (1978). Paper presented at the National Conference on Crystallography, Sardar Patel University, Vallabh Vidya Nagar, February.

LAL, K., SINGH, B. P. & VERMA, A. R. (1978). Paper presented at the IVth International Conference on Vapour Growth and Epitaxy, Nagoya, Japan, July 9–13.

LAL, K., SINGH, B. P. & VERMA, A. R. (1979). *Acta Cryst.* A**35**, 286–295.

LAL, K., SINGH, B. P., VERMA, A. R. & SCHWUTTKE, G. H. (1978). *Acta Cryst.* A**34**, S273.

PATEL, J. R. (1973). *J. Appl. Phys.* **44**, 3903–3906.

PATEL, J. R. (1975). *J. Appl. Cryst.* **8**, 186–191.

PATEL, J. R. & BATTERMAN, B. W. (1963). *J. Appl. Phys.* **34**, 2716–2721.

PEISL, H. (1975). *J. Appl. Cryst.* **8**, 143–149.

PEISL, H. (1976). *Defects and their Structure in Non-Metallic Solids*, edited by B. HENDERSON & A. E. HUGHES, pp. 381–404. London, New York: Plenum.

SCHWUTTKE, G. H. (1962). *Direct Observation of Imperfections in Crystals*, edited by J. B. NEWKIRK & J. H. WERNICK, pp. 497–508. New York: Interscience.

SCHWUTTKE, G. H. (1970). *Crystal Properties as Influenced by Crystallographic Imperfections*, Ch. 1. IBM Ref. No. TR 22.978.

TRINKAUS, H. (1971). *Z. Angew. Phys.* **31**, 229–235.

TRINKAUS, H. (1972). *Phys. Status Solidi B*, **51**, 307–319.